Analysis of Antimonide-Based Interdiffused Quantum Wells

Steven K. H. Sim[a], E. Herbert Li[a], Kabula Mutamba[b] and Hans L. Hartnagel[b]

[a]Department of Electrical and Electronic Engineering, University of Hong Kong, Pokfulam Road, Pokfulam, Hong Kong

[b]Institut fuer Hochfrequenztechnik, Technische Universitaet Darmstadt, Merckstrasse 25, 64283 Darmstadt, Germany

ABSTRACT

Antimonide(Sb) is said to be an emerging optoelectronic material for both high speed and long wavelength electronics devices. Recently, there has been much research activities on antimonide based system. Among Group V elements, antimonide is of particular interest as its lattice parameter matches solid solutions of various ternary and quarternary $III-V$ compounds whose band gap cover a wide spectral range from absorption in antimonide based superlattices, detection of longer wavelength of 8 to 14μm is possible. With the technique of interdiffusion applying to an antimonide based quantum well, we will be able to obtain devices which are bias tunable. This technique of interdiffusion is a thermal process which induces an interdiffusion of the constituent atoms across the heterointerfaces of an as-grown quantum well, and results in modification of the composition and confinement profiles of the quantum well structures. Hence, the optical properties of the material can be modified to desire values. In this presentation, an antimonide based interdiffused quantum well structure is carefully examined including experimental results, with strong emphasis on its tunable properties and summerized with focus on its device applications and future development.

Keywords: Antimonide, Interdiffusion, Quantum Well, Mid-Infrared Absorption

1. INTRODUCTION

The search of suitable materials for infrared (IR) detection has been carried out since 1800, right after the initial discovery of infrared radiation by Herschel.[1] From time to time, materials such as Tl_2S, PbS, $InSb$, and $HgCdTe$ have become a research target for infrared detection applications. The $HgCdTe$ infrared detector is one of the most commonly used and most commercially available detectors today.[2] Although these detectors have been around for a long time and many paper were published on them, they still, like all bulk material detectors, suffer from a disadvantage due to the limitation of their achievable wavelengths. The latter is defined by the band gap of the detection material. Since the material band gap cannot be adjusted for a bulk material with a defined composition, the operating wavelength of such detectors can only reach a certain value.

Because of the availability of infrared detectors, two atmospheric windows have been identified to be useful in some applications. The two atmospheric windows are defined as medium wavelength infrared region (MWIR, $3-5\mu$m), and long wavelength infrared region (LWIR, $8-12\mu$m). It is known that when an object heated to around $300K$ will have an emission peak at about 10μm in the LWIR. As the temperature of an object increases to around $700K$ and $800K$, the emission peak will be shifted to the MWIR. Because of this, both the biomedical and military sectors have put a huge effort in developing and improving infrared detection system. Research of infrared technology for peace-time military applications in terms of surveillance and for environmental sensing has grown tremendously over the past few years. This is due to the following advantages of infrared properties. Firstly, thermal radiation of non-zero temperature objects lies in the infrared region. This is particular useful for target detection in cluster environment. Secondly, infrared systems are not easily counter-detected. Both of this properties are ideal for target tracking and surveillance applications. This detection scheme can work in a noisy environment. There has been a third atmospheric detection window found, which lies at around 20μm. It is very useful for aerospace applications in remote sensing and space telescopes.

As the development of quantum well (QW) is becoming more and more mature, one of the successful application of these quantum structure is QW infrared photodetector (QWIP). Currently, two types of QWIP are used. One is

Other author information: (Send correspondence to E. Herbert Li)
E. Herbert Li: E-mail: ehli@eee.hku.hk

Part of the SPIE Conference on Optoelectronic Materials and Devices • Taipei, Taiwan • July 1998
SPIE Vol. 3419 • 0277-786X/98/$10.00

based on the intersubband absorption and the other is based on the interband absorption. The operating principle of intersubband transition detectors is based on the optical transition within the same energy band, also known as intersubband transition.[3] Another type is the one base on coventional interband transition from valence to conduction bands. Hence, the band gap of the detecting material is no longer the limiting factor of longer wavelength detector. For the intersubband absorption system, both type I and type II QW structures can be used. The transition energy is determined by the first and the second energy levels. Common design is to construct a QW where the second energy levels is either near the top or just above the barrier. Interband absorption can occur in type I QW (valence band to conduction band vertical transition) or in type II QW (via phonon exchange). The interband transition energy of the type II structure is determined by the band gap between the first valance energy level in the barrier and the first conduction energy level in the well. These energy levels can be tailored by carefully designing the QW structural parameters. Ideally speaking, both of these systems are unlimited in their operating wavelengths.

In this paper, we present a model of all the subband bound states and a number of continuum states in an undoped $Al_xIn_{1-x}Sb/InSb$ interdiffused single quantum well, with emphases on its infrared detection applications. In section 2, we briefly describe the model that we used to obtain our subband energy levels. Section 3 presents the results and a discussion on the implication of its applicaiton in QWIPs. Finally, the main results of this paper are summarized in the conclusion.

2. THEORETICAL MODEL

The quantum well structure modeled in this paper is an $Al_xIn_{1-x}Sb/InSb$ single quantum well. The QW is assumed to be undoped, and the effects of unintentional impurities are also ignored. For numerical efficiency, the barrier width of the quantum well is assumed to be infinitely thick and is approximated by a large finite barrier width.

The diffusion process is characterized by a diffusion length L_d, which is defined as[4]:

$$L_d = (D \times t)^{\frac{1}{2}} \tag{1}$$

where D and t are the diffusion coefficient and the annealing time, respectively. In the model presented here, we assume an isotropic interdiffusion of Al with a constant diffusion coefficient independent of Al concentration, i.e., according to Fick's second law of diffusion.[5]

The Al composition profile, $\tilde{w}(z)$, across the quantum well structure is given by[6]

$$\tilde{w}(z) = w_0\left\{1 - \frac{1}{2}\left[erf\left(\frac{L_z + 2z}{4L_d}\right) + erf\left(\frac{L_z - 2z}{4L_d}\right)\right]\right\}, \tag{2}$$

where w_0 is the as-grown Al mole fraction in the barrier, L_z is the as-grown width of the quantum well, z is both the quantization and the growth axis and $erf()$ is error function.[7] Equation (2) is used to obtain the $\tilde{E}_g$, the well-barrier discontinuity $\Delta\tilde{E}_g$, and the well depth $\Delta\tilde{E}_r$, which are defined as follows:

$$\begin{aligned} \tilde{E}_g(z) &= E_g(w = \tilde{w}(z)), \\ \Delta\tilde{E}_g &= E_g(w_0) - \tilde{E}_g(z = 0), \\ \Delta\tilde{E}_r &= Q_r \times \Delta\tilde{E}_g, \end{aligned}$$

where the subscript r denotes either the electron in the conduction band (C), or heavy or light holes in the valance band ($V = H$ or L). The interdiffusion-induced quantum well confinement profile $U_r(z)$ is defined by

$$U_r(z) = Q_r[\tilde{E}_g(z) - \tilde{E}_g(z = 0)]. \tag{3}$$

We have defined the zero potential to be at the bottom ($z = 0$) of the interdiffused QW and positively up in both bands except for valence subband mixing, which is taken to be negative down; the absolute position of this zero potential varies with diffusion length, L_d and the band offset splitting, Q_r. The crossover point (COP) potential $U_{COP\cdot r}$ is defined as

$$U_{COP\cdot r} = Q_r[\tilde{E}_g(z = \frac{1}{2}L_z) - \tilde{E}_g(z = 0)], \tag{4}$$

which is the potential at the two identical intersections of the as-grown and the diffused potential profiles at $z = \pm\frac{1}{2}L_z$, and is measured positively up from the bottom of the confinement profile for both bands.

The valence subband structure is described by a multiband effective-mass approximation based on the $k \cdot p$ method of Lüttinger and Kohn.[8] The low lying conduction subband states are assumed to be almost purely s-like and nondegenerate, while the low lying under subband states are almost purely p-like and four fold degenerate. The slowly varying part of the subband states are described by the envelope function scheme. The non-interacting electron and hole states are thus described by

$$\Psi_C(k_{\|}, z) = \Psi_C(z)u_{0C}(\Gamma)e^{ik_{\|}\cdot\rho} \tag{5}$$

and

$$\Psi_V(k_{\|}, z) = \Psi_V(k_{\|}, z)u_{0V}(\Gamma)e^{ik_{\|}\cdot\rho}, \tag{6}$$

respectively, where the u_0's are the zone-center Bloch functions for the bulk materials; Ψ's are the envelope functions for the quantum-well confinement; $k_{\|} = (k_x, k_y)$ is the transverse (in-plane) wave vector which is in the direction parallel to the plane of the quantum-well layer and perpendicular to the z axis; $r = r(x, y, z)$, and $\rho = \rho(x, y)$.

Using Ben-Daniel and Duke model,[9] the electron and holes at the zone center of Γ_6-valley symmetry can be calculated separately, with a z-position dependent effective mass on the interdiffused composition profile. The one-dimensional Schrödinger-like equation, for the envelope function $\Psi_{rl}(z)$, is then written as follows:

$$-\frac{\hbar^2}{2}\frac{d}{dz}\left[\frac{1}{m^*_{\perp r}(z)}\frac{d\Psi_{rl}(z)}{dz}\right] + U_r(z)\Psi_{rl}(z) = E_{rl}\Psi_{rl}(z), \tag{7}$$

where $l = 1, 2, \ldots$ are the quantum-well subband levels for either the electrons (Cl) or holes (Vl), respectively; $m^*_{\perp r}(\tilde{w}(z))$ is the carrier effective mass in the z direction; $E_{rl} \equiv E_{rl}(k_{\|} = 0)$ is the subband-edge energy, and the origin of the potential energy is taken at the bottom of the error function profile quantum-well. Equation (7) is solved numerically using finite difference method with the confinement profile defined in Equation (3) and the boundary conditions are taken to be zero at the end of a finite and large barrier $[\Psi_{rl}(\pm z_f) = 0]$; in other words, the error function profile quantum-well (EFQW) is embedded in a well of width $L_f = 2z_f$ with an infinitely high barrier to approximate the thick barrier.

For finite $k_{\|} \neq 0$, the electron non-parabolic in-plane dispersion can be modeled by a fourth-order expansion with the coefficients (α_0 and β_0) determined using a 14 band $k \cdot p$ calculation.[10] Neglecting the spin-orbit splitting term and keeping only an anisotropic fourth-order term, the dispersion energy can be expressed as

$$E_C(k) = \alpha_0 k_z^4 + \frac{\hbar^2}{2m^*_c}(k_z^2 + k_{\|}^2) + (2\alpha_0 + \beta_0)k_z^2 k_{\|}^2. \tag{8}$$

Two anisotropic quantum-well masses in the confinement and in-plane directions can be derived and expressed as

$$m^*_{\perp C}(E_{Cl}, w) = m^*_C(w)\frac{[1 - (1 - 4\alpha E_{Cl})^{\frac{1}{2}}]}{2\alpha E_{Cl}} \tag{9}$$

and

$$m^*_{\| C}(E_{Cl}, w) = m^*_C(w)[1 + (2\alpha + \beta)E_{Cl}], \tag{10}$$

respectively.

It is more difficult to solve the valence subband dispersion, since coupling mixes the heavy and light hole states for $k_{\|} \neq 0$, thus preventing the diagonalization of the fourfold degenerate Lüttinger Hamiltonian which can be solved using an effective Hamiltonian developed by Chan.[11] This approach is based on the analogous application of the $k \cdot p$ method to the subbands. Equation (5) is an approximation of the coupled envelope fucntion $\Psi_V(k_{\|}, z)$ in Equation (6) at $k_{\|} = 0$. It is sufficient for a small range of $k_{\|}$ at near 0 to study the properties of the quantum-well, as the quantum-well effects only manifest themselves near to the zone-center subband edge. The basis for the expansion is defined as follows:

$$\Psi(k_{\|}, z) = \sum_{l=1}^{N}\sum_{V=-3/2}^{3/2} d_{V,l}(k_{\|})\Psi_{V,l}(z), \tag{11}$$

where V is running over the lifted fourfold degenerate holes states and N is the maximum number of bases taken in each V, and the effective Hamiltonian is

$$\begin{bmatrix} E_{3/2} & C & B & 0 \\ C^* & E_{-1/2} & 0 & B^T \\ B^* & 0 & E_{1/2} & C^T \\ 0 & B^* & C^* & E_{-3/2} \end{bmatrix}, \tag{12}$$

where

$$C_{ll'} = \left[\frac{3}{4}\right]^{\frac{1}{2}} \frac{\hbar^2}{m_0}\gamma_2(k_x - ik_y)^2 \int_0^{L_f} dz \psi_{-3/2,l}(z)\Psi_{1/2,l'}(z), \tag{13}$$

$$B_{ll'} = 3^{\frac{1}{2}} \frac{\hbar^2}{m_0}\gamma_2(-k_x - ik_y) \int_0^{L_f} dz \Psi_{3/2,l}(z)\frac{\partial}{\partial z}\Psi_{-1/2,l}, \tag{14}$$

$$E_{\pm 3/2,ss'} = \delta_{ss'}E_{Hs} - \frac{\hbar^2}{2m_{\parallel H}}k_{\parallel}^2, \tag{15}$$

$$E_{\pm 1/2,ss'} = \delta_{ss'}E_{Ls} - \frac{\hbar^2}{2m_{\parallel L}}k_{\parallel}^2, \tag{16}$$

$\gamma_2(w)$ is the Lüttinger parameter, and L_f is the width of a square quantum well with infinitely high barriers which contains the EFQW. The introduction of this larger well is to numerically determine the continuum levels above the top of the EFQW. It should be noted that, in the absence of an applied electric field or any other mechanism that will distort the inversion symmetry assumed here, the symmetric EFQW confinement potential profile causes the valence subband to exhibit a twofold Kramer's spin degeneracy.

3. RESULTS AND DISCUSSIONS

The model which has been used to calculate the subband edge energies of our QW structure has already been discussed in the last section. The parameters used in our subband calculations are presented in Table 1. The material parameters of binary Sb-based compounds were obtained from experimental results, and the AlInSb ternary material parameters were obtained from linear interpolation of the InSb and AlSb parameters. Only room temperature data were considered in the model.

In our model, we consider a $Al_xIn_{1-x}Sb/InSb$ QW with Al-mole fraction varing between $x = 0.08$ and $x = 0.25$. The QW width is fixed at 70Å, no electric field were applied, and the entire structure is undoped. In Table 2, we present the subband energies of $Al_{0.25}In_{0.75}Sb/InSb$ QWs. As it can be seen, the subband level is increasing initially as diffusion length increases and then decreases at larger diffusion lengths. This is due to a narrower effective well width created in the beginning of interdiffusion and a widening of the well at a more extensive stage of interdiffusion. Bulk band gap at well center also increases, and the well depth for both conduction and valences band decreases. In the case of $L_d \to \infty$, the quantum well structure becomes a bulk material.

The interband transition energy, E_{11H}, of a interdiffused QW is defined by $E_{11H} = \tilde{E}_g + E_{1C} + E_{1H}$, where $\tilde{E}_g$ is the bulk band gap of the well material, E_{1C} and E_{1H} is the first subband energy of conduction and heavy hole respectively. It is noted that the heavy hole and light hole were split apart. This is due to both the QW confinement and the strain induced by the lattice mismatch between these barrier and the well materials. The compressive strain induced is in the QW structure causing the heavy hole to move towards the the conduction band and light hole moves in the opposite direction. The lattice constant of $InSb$ is larger than that of $Al_{0.25}In_{0.75}Sb$ and the QW is grown on the top of a $GaSb$ substrate, which is one of the common substrate used for antimonide-based QW. However, the lattice of $GaSb$ does not match that of the barrier material. Therefore, we introduce a buffer layer region in between the barrier and the substrate to accomodate the lattice mismatch. This buffer layer is made up of $In_xGa_{1-x}Sb$, as it is shown in Figure 1. $In_xGa_{1-x}Sb$ and $Al_yIn_{1-y}Sb$ can, at certain x and y values, be grown one another lattice matched. Hence, we this buffer layer can be introduced in a form of a grading with the In concentration gradually increasing from the zero at the GaSb substrate to that of the barrier material. The QW structure is then grown on top of the buffer layer, this will induce a compressive strain in the well material. The schematics of the QW structure is presented in Figure 2.

Parameters	$Al_xIn_{1-x}Sb$	*Unit*	*Reference*
$Q_c : Q_v$	$0.76 : 0.24$		
$E_g(x)$	$0.17 + 1.7x + 0.43x^2$	eV	12,13
$\Delta_0(x)$	$0.81 - 0.06x$	eV	14,15
$\frac{dE_g}{dp}$	$15.7 - 17.3x$	$10^{-6}eVkg^{-1}$	13,16
$\gamma_1(x)$	$35.08 - 30.93x$	m_0	17,16
$\gamma_2(x)$	$15.64 - 14.63x$	m_0	17,18
$\gamma_3(x)$	$16.91 - 15.16x$	m_0	17,16
$m_c^*(x)$	$0.0135 + 0.0965x$	m_0	13,14
$m_{\parallel L}^*(x)$	$0.015 + 0.108x$	m_0	19,20
$m_{\parallel H}^*(x)$	$0.263 + 0.073x$	m_0	21,19
$\epsilon(x)$	$17.76 - 6.548x$	ϵ_0	16,15
$\alpha(x)$	$1.8x - 7.7$	eV^{-1}	22,16
$\beta(x)$	$0.6x - 2$	eV^{-1}	23,16
c_{11}	$6.669 + 2.1x$	$10^{11}dyncm^{-2}$	16,19
c_{12}	$3.645 + 0.696x$	$10^{11}dyncm^{-2}$	16,19
a_0	$6.47937 - 0.34337x$	$\AA$	16,19

Table 1. Material parameters of $Al_xIn_{1-x}Sb$; m_0 and ϵ_0 are respectively the electron mass and static dielectric constant of the free space.

Subband	*Subband-edge energy (meV)*							
Level	$L_d = 0$	$L_d = 5$	$L_d = 10$	$L_d = 15$	$L_d = 20$	$L_d = 25$	$L_d = 30$	$L_d = 35$
C_1	108.2	104.6	110.6	101.8	85.3	70.0	57.7	48.2
C_2					219.3	183.8	153.7	129.8
$Depth_C$	276.7	276.7	273.4	252.1	222.3	194.5	171.2	152.1
H_1	17.8	19.8	25.8	25.7	21.9	17.9	14.7	12.3
H_2	68.5	72.2	79.9	74.1	62.1	50.9	42.0	35.1
H_3	137.1	133.5	127.6	112.1	93.3	76.9	64.0	53.9
$Depth_H$	142.9	142.9	141.0	129.2	113.0	98.1	85.8	75.8
L_1	19.7	19.7	18.0	17.1	15.6	14.0	12.4	11.0
$Depth_L$	24.9	24.9	24.8	24.3	23.2	21.6	19.9	18.4

Table 2. Subband-edge energies, measured from the bottom of the interdiffused $Al_{0.25}In_{0.75}Sb/InSb$ quantum-well structure. The well width is $70\AA$, and L_d varies between zero and $35\AA$.

This QW structure is highly strained, since the lattice mismatch between barrier and well materials is relatively high. A Lattice mismatch of less than 2% is generally accepted for QW structures without strain relaxation and creation of defects. Because of strain, the well thickness of a QW is also an important factor to be considered, since this thickness determines the limit of strain relaxation. In table 3, we present the percentage of lattice mismatch, critical layer thickness, well material bulk band gap and interband transition energy of square QWs with different *Al* mole fractions. Interdiffused QW is not considered in this table, since interdiffusion can reduce the lattice mismatch between barrier and well, and critical layer thickness increases in value. The well material bulk band gap has changed over different *Al* mole fractions at the barrier. The main reason for this is due to the compressive strain induced in the well. The compressive strain will cause a widening of the band gap. Therefore, the band gap changes even for the same QW material structure.

The interband transition energy determines the peak interband absorption, and which then defines the operation wavelengths of the QWIP. The interband absorption wavelength versus diffusion length for different *Al* mole fractions are shown in figure 3. The effect of interdiffusion on the change of transition energy is much more obvious at higher *Al* mole fractions. It gives a high tunnability of such QWIPs. However, the transition energy of square QWs is much

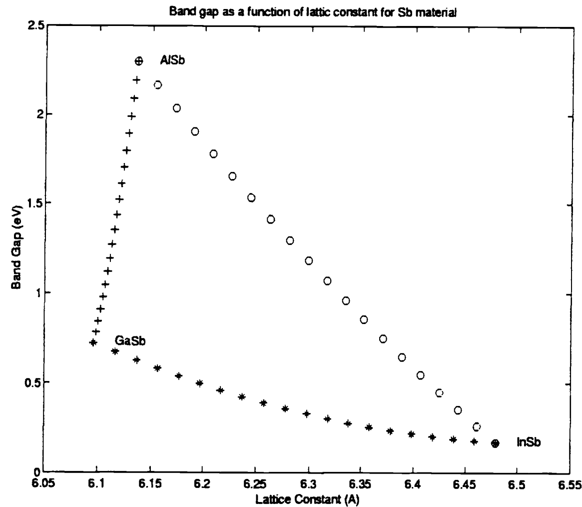

Figure 1. Band gap as a function of lattice constant for Sb-based materials.

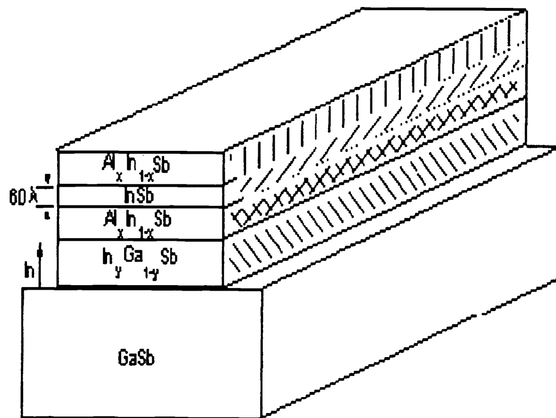

Figure 2. Schematic diagram of the $Al_xIn_{1-x}Sb/InSb$ quantum well structure.

larger than that at small Al mole fractions. Vice versa at small Al mole fractions, a smaller interband transitions energy can be achieve, but the interdiffusion does not give a good tunability.

As we can see from Figure 3, the modeled QW structure covers the MWIR. Hence, it demonstrates the feasibility of medium infrared detectors design based on the Sb-based material system. The use of the intersubband transitions in type-I QW offers the advantage of direct absorption with a wide mid-infrared wavelength range. By carefully designing, an interdiffused QWIP array can be built to detect infrared wavelengths between $3 - 5\mu m$. We have also determined the QW absorption coefficient for $Al_{0.25}In_{0.75}Sb$ with different diffusion length under both TE and TM polarization. The corresponding results are respectively presented in Figures 4 and 5. However, absorption of bulk material at the barrier and the substrate were not considered, since the bulk material absorption energy is much higher than that of the QW. No account has been taken of the excitonic contribution to the absorption. It is expected the exciton binding energies should be small due to the low electron mass in $InSb$.

	Al mole fractions				
	$Al_{0.08}$	$Al_{0.10}$	$Al_{0.15}$	$Al_{0.20}$	$Al_{0.25}$
Lattice Mismatch (%)	0.42	0.53	0.79	1.06	1.32
Critical Layer Thickness ($\AA$)	301	228	136	94	69
Well Material Bulk Band Gap (meV)	180.4	182.9	189.6	195.8	202.3
Interband Transition Energy (meV)	251.4	264.2	290.1	310.8	328.3

Table 3. Percentage of lattice mismatch, critical layer thickness, well material bulk band gap and interband transition energy at different Al mole fractions of a $Al_xIn_{1-x}Sb/InSb$ square QW.

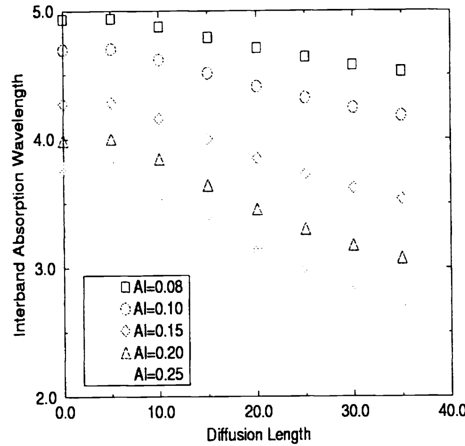

Figure 3. Interband absorption wavelength for various Al concentration of the $Al_xIn_{1-x}Sb/InSb$ QW.

In addition to the interband absorption wavelengths between $3-5\mu$m, there are others intersubband wavelength ranges. These are based on the same QW structure with $Al_{0.25}In_{0.75}Sb$ barrier (gives λ between $8-12\mu$m) and $Al_{0.15}In_{0.85}Sb$ barrier (gives λ around 20μm). In both cases, the second conduction subband level is just above the QW. After some QW interdiffusion, the second conduction subband level will be pulled down to just underneath the top of the barrier. The third conduction subband level is always high above the barrier in the system that we design. Hence, with the same material system, a long wavelength far-infrared photodetector can be realized.

In this analysis, we have proposed using $Al_xIn_{1-x}Sb/InSb$ for the QWIP to operate at $3-5\mu$m. However, the major purpose of our model is to calculate the subband edge energies level and other absorption coefficients for an interdiffused QW. Before fabricating any QWIP from this material design, it is essential to construct another model to fully examine the detector performance. This includes factors like photoconductivity gain, responsivity, dark current and noise.

4. CONCLUSION

This paper has presented a study on the subband edge energies level for $Al_xIn_{1-x}Sb/InSb$ interdiffused QW. The results show that by using such QW structures, the subband levels can be controlled. Due to the narrowness of the $InSb$ band gap, it is also possible to design a type-I interband QWIP via direct transitions between the valence and conduction bands. As it is shown in our calculation, by applying the interdiffusion technique to the QW, it is possible to tune the QW interband transition energy to a desired value. In our results, we have shown that, by varying the Al concentration from 0.08 to 0.25, interband absorption wavelengths in the medium infrared region can be obtained. This type of QW can also be used for a type I intersubband absorption QWIP schemes. With careful

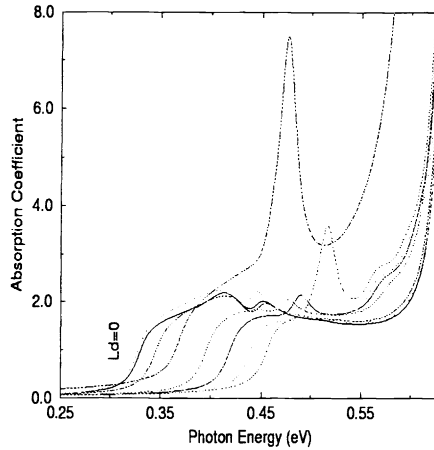

Figure 4. *TE* Absorption Coefficient for different diffusion lengths.

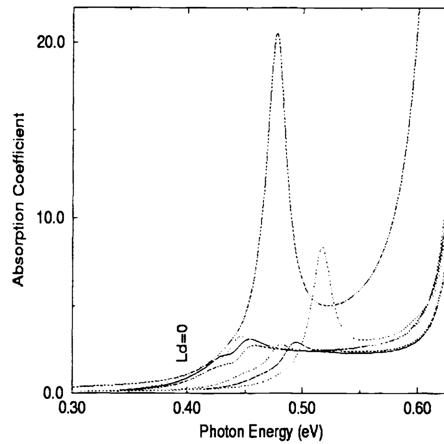

Figure 5. *TM* Absorption Coefficient for different diffusion lengths.

design, detection of $8-12\mu m$ and $20\mu m$ radiation can be achieved. However, many factors affecting the performance of detectors have not been considered here. It is necessary to construct a model to calculate these factors in order to confirm the advantage of using $Al_xIn_{1-x}Sb/InSb$ interdiffused QWIP.

ACKNOWLEDGMENTS

This work was supported in part by the RGC earmarked grant of Hong Kong, the University of Hong Kong CRCG research grant and the DAAD-RGC grant between Hong Kong and Germany.

REFERENCES

1. M. Razeghi, *Long Wavelength Infrared Detectors*, Gordon and Breach Science, Amsterdam, Netherlands, 1996.
2. A. Rogalski, *Infrared Photon Detectors*, SPIE Optical Engineering Press, Washington, USA, 1995.

3. M. O. Manasreh, *Semiconductor Quantum Wells and Superlattices for Long-Wavelength Infrared Detectors*, Artech House, Boston, London, 1993.
4. K. Kash, B. Tell, P. Grabbe, E. A. Dobisz, H. G. Graighead, and M. C. Tamargo *J. Appl. Phys.* **63**, p. 190, 1988.
5. J. Crank, *The Mathematics of Diffusion, 2nd ed*, Oxford University, Oxford, 1975.
6. T. E. Schlesinger and T. Kuech *Appl. Phys. Lett.* **49**, p. 519, 1986.
7. M. Abramowitz and I. A. Stegun, *Handbook of Mathematical Functions*, National Bureau of Standards, Washington, DC, 1964.
8. J. M. Luttinger and W. Kohn *Phys. Rev.* **97**, p. 869, 1955.
9. D. J. Ben-Daniel and C. B. Duke *Phys. Rev.* **152**, p. 638, 1966.
10. U. Ekenberg *Phys. Rev. B* **40**, p. 7714, 1989.
11. K. S. Chan *J. Phys. C.* **19**, p. L125, 1986.
12. A. Joullie, B. Girault, A. M. Joullie, and A. Zien-Eddine *Phys. Rev. B* **25**, p. 7830, 1982.
13. Pankove and I. Jacques, *Optical processes in semiconductors*, Prentice-Hall, 1971.
14. M. Levinshtein, S. Rumyantsev, and M. Shur, *Handbook series on semiconductor parameters*, World Scientific, Vol 2.
15. P. P. Paskov, "Refractive-indexes of InSb, InAs, GaSb, $InAs_xSb_{1-x}$, and $In_{1-x}Ga_xSb$ - effects of free-carriers," *J. Appl. Phys.* **81**, pp. 1890–1898, 1997.
16. O. Madelung, M. Schulz, and H. Weiss, *Landolt-Börnstein, Numerical Data and Functional Relationships in Science and Technology*, Springer, New York, 1982.
17. P. Thomas and Pearsall, *Strained-Layer Superlattices : Physics*, Academic Press, 1990.
18. E. R. Heller, K. Fisher, F.Szmulowicz, and F. L. Madarasz, "Superlattice parameters for optimum absorption in $InAs/In_xGa_{1-x}Sb$ superlattice infrared detectors," *F-Bnzllzua-tevg* **77**, pp. 5739–5746, 1995.
19. O. Madelung, *Semiconductor - Basic Data*, Springer, New York, 1996.
20. M. Levinshtein, S. Rumyantsev, and M. Shur, *Handbook series on semiconductor parameters*, World Scientific, Vol 1.
21. C. H. Yu, Y. K. Su, and F. S. Juang, "GaSb/InGaSb strained-layer quantum wells by MOCVD," *Solid State Electronics* **35**, pp. 1385–1390, 1992.
22. V. Swaminathan and A. T. Macrander, *Materials aspects of GaAs and InP based structures*, Prentice-Hall, 1991.
23. M. E. Flatte, C. H. Grein, H. Ehrenreich, R. H. Miles, and Cruz, "Theoretical performance limits of $2.1-4.1\mu m$ InAs/InGaSb, HgCdTe, and InGaAsSb lasers," *J. Appl. Phys.* **78**, pp. 4552–4559, 1995.